Lotus: Rethinking Polarization Mismatch for Carrier Cancellation in Backscatter Systems

Xiuzhen Guo, *Member, IEEE*, Long Tan, *Student Member, IEEE*, Yuan He, *Senior Member, IEEE*, Yuanchao Shu, *Senior Member, IEEE*, and Jiming Chen, *Fellow, IEEE*

***Abstract*—Carrier interference is a fundamental research challenge in backscatter systems. Existing solutions leverage frequency shifting or full duplex designs to mitigate carrier interference in the analog or digital domain. However, these solutions introduce extra spectrum usage, protocol overhead, and power consumption, all of which are undesirable in backscatter systems. In this paper, we revisit polarization mismatch and propose Lotus, a low-cost analog design to combat carrier interference for backscatter systems. Lotus comprises a novel antenna design and a backscatter tag design. At runtime, Lotus antenna replaces the receiver default antenna to cancel out the carrier interference, without any protocol or hardware overhead. Lotus tag mitigates the power loss caused by polarization mismatch and remains compatible with all existing backscatter radios. Experimental results show that Lotus achieves comparable cancellation gain (i.e., 42 dB) with the state-of-the-art frequency-shifting baseline. Meanwhile, Lotus outperforms the baseline by $2\times$ and $6.5\times$ in spectrum and power efficiency, respectively. Additionally, Lotus achieves comparable performance to the frequency shifting baseline regarding backscatter range and throughput across three backscatter technologies, including Wi-Fi, Bluetooth, and LoRa.**

***Index Terms*—Wireless networks, backscatter communication, LoRa, antenna.**

I. Introduction

DUE to the ultra-low-power, low-cost, and small form factor, backscatter radio has emerged as a promising communication solution for the Internet of Things (IoT) [1], [2]. Despite the remarkable technological advancement, backscatter still faces a fundamental challenge: *carrier interference*. This interference significantly diminishes communication range and throughput, as the weak backscatter signal often gets drowned out by the carrier signal transmitting in the same frequency (Figure 1). The low signal-to-interference plus noise ratio (SINR) sets a strong barrier to backscatter decoding.

Received 25 October 2024; revised 18 July 2025; accepted 5 January 2026; approved by IEEE TRANSACTIONS ON NETWORKING Editor T. Zhu. Date of publication 12 January 2026; date of current version 19 January 2026. This work was supported in part by the National Science Fund of China under Grant 62472379, Grant 62425207, Grant 62394341, Grant 62394344, and Grant 92467301; in part by Zhejiang Provincial Natural Science Foundation of China under Grant LR26F020001; and in part by the Key Research and Development Program of Zhejiang Province under Grant 2025C01012. *(Corresponding author: Yuan He.)*

Xiuzhen Guo, Long Tan, Yuanchao Shu, and Jiming Chen are with Zhejiang University, Hangzhou 310027, China (e-mail: guoxz@zju.edu.cn; long.tan@zju.edu.cn; ycshu@zju.edu.cn; cjm@zju.edu.cn).

Yuan He is with Tsinghua University, Beijing 100084, China (e-mail: heyuan@mail.tsinghua.edu.cn).

Digital Object Identifier 10.1109/TON.2026.3652168

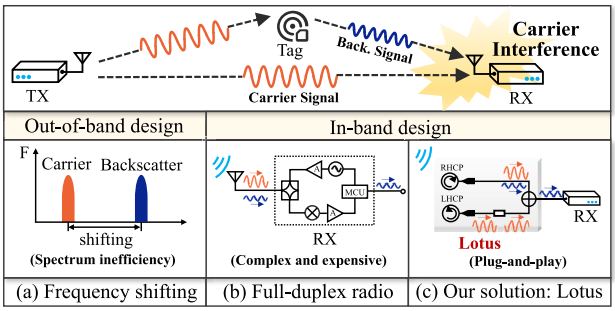

Fig. 1. Comparison of different carrier cancellations.

To mitigate the carrier interference, existing in-band backscatter systems (e.g., RFID reader [3], BackFi [4], Full Duplex LoRa [5]) adopt full-duplex radio designs [6], [7] to cancel out the carrier interference. However, these hardware (*i.e.* analog) cancellation solutions are hardware-specific and introduce extra costs. The alternative digital cancellation designs [8], [9] require access to IQ samples, commonly unavailable on commodity devices. Other works [10], [11], [12] adopt the frequency-shifting technique to achieve out-of-band backscatter, thus avoiding carrier interference. However, generating a frequency-shifting signal aggravates the power burden at the tag because the power consumption scales with the clock frequency. These approaches also introduce additional wireless spectrum usage and deployment overhead.

As backscatter systems aim for long-term, low-power, and ubiquitous deployment, it is critical to find a spectrum-efficient, cost-effective, and low-overhead solution for carrier interference cancellation. Diverging from aforementioned approaches, we explore an overlooked attribute of backscatter signals: polarization. The polarization of an electromagnetic wave emitted from an antenna delineates the geometric orientation of its oscillations. When the polarization angle of a signal aligns with that of the receiver antenna, the received signal power reaches its maximum. Conversely, when the polarization angle of the signal is orthogonal to that of the receiver antenna, the receiver can hardly receive the signal. Therefore, by maximizing the polarization alignment between the backscatter signal and the receiver antenna while minimizing the alignment between the carrier signal and the receiver antenna, we can effectively eliminate carrier interference while retaining the backscatter signal.

However, embracing such a paradigm is challenging in backscatter systems, primarily due to unstable cancellation gain. To maximize the carrier cancellation gain, it is crucial to ensure the polarization of the receiver antenna is always in perpendicular to the carrier antenna. Unfortunately, the polarization angle of the carrier antenna is not always stable in real-world applications such as warehouse inventory and supply chains, thus deteriorating the polarization mismatch between the receiver and carrier antennas. Performing ad-hoc calibration for polarization mismatch with each carrier angle is difficult for the receiver. Furthermore, the polarization angle of the carrier signal is significantly affected by multipath effects. Consequently, leveraging polarization mismatch for carrier interference cancellation achieves desirable performance on the millimeter band where the tag-to-receiver distance is relatively short [13]) and is far from application in current backscatter systems.

In this paper, we revisit the polarization mismatch and introduce Lotus. Lotus consists of a tag design and a receiver antenna design. Different from existing carrier cancellation approaches, the Lotus tag is applicable to any linearly polarized carrier antenna, and the Lotus antenna is compatible with existing backscatter receivers without any software or hardware modifications. By simply replacing the default antenna on the receiver with Lotus, the backscatter receiver consistently achieves high levels of carrier cancellation gain (around 42 dB). Lotus achieves plug-and-play, calibration-free, low-cost, and low-power carrier cancellation capability through the following design features.

• **On-antenna carrier signal cancellation (§ IV).** Lotus takes advantage of destructive interference to cancel out the strong carrier signal at the analog domain. We propose an integrated patch coupled with a quadrature hybrid that constructs a pair of right-hand circularly polarized (RHCP) port and left-hand circularly polarized (LHCP) port. The LHCP and RHCP are orthogonal and can both receive the incident carrier signal. *Once received by the RHCP and LHCP ports, the incident carrier signal after microstrip lines no longer has polarization characteristics, but is transformed into two identical electrical signal copies with the same amplitude, frequency, and phase.*[1] These two copies then pass through a 180° hybrid and add destructively at the output port to cancel each other.

• **On-tag backscatter signal amplitude compensation (§ V).** To survive the backscatter signal at the Lotus antenna, our backscatter tag transforms the linearly polarized carrier into an RHCP backscatter signal. Upon arriving at the receiver antenna (*i.e.*, Lotus antenna), the RHCP backscatter signal will pass through only the RHCP chain at the receiver and thus would not be canceled out at the combiner. However, there will be a 3 dB loss due to the polarization mismatch between the linearly polarized carrier signal and the circularly polarized backscatter antenna. Inspired by TunnelScatter [14], [15], our tag design takes advantage of the tunnel diode to compensate for this 3 dB loss. As the amplification gain of the tunnel diode is hyper-sensitive to the power of the incident signal (which is determined by the spacing between the tag and the carrier generator), we further propose an impedance adaptation algorithm to manipulate the power of the carrier to ensure the tunnel diode never turn into an attenuator.

• **Implementation**. We prototype both 2.4 GHz and 915 MHz Lotus antenna using the aluminum alloy material with 8.5 mm thickness. The antenna gain is 3 dBi. The material and manufacturing costs are around 5 USD and 16 USD, respectively. The size, weight, and price are expected to be significantly reduced after mass production. We further prototype Lotus tag on a $60\,\text{mm} \times 40\,\text{mm}$ one-layer Printed Circuit Board (PCB) using commercial off-the-shelf circuit components. The Lotus backscatter front-end can be easily integrated into existing backscatter tag designs with around $70\ \mu$W extra power consumption. The Application Specific Integrated Circuit (ASIC) can further reduce power consumption sharply.

Our contributions are summarized below.

(i) We systematically study the polarization mismatch property of electromagnetic waves for carrier cancellation and propose a novel hardware solution that is low-cost, scalable, and resilient to multi-path effects. It works with the linearly polarized carrier signals without any software modification or hardware upgrading to the receiver.

(ii) We address critical design and implementation challenges spanning the Lotus antenna and tag. We further propose a plug-and-play tag and front-end module that can easily adapt to existing backscatter radio designs with ignorable engineering efforts.

(iii) Owing to the carrier cancellation gain brought by the Lotus antenna and the amplification gain brought by the tag, our evaluation shows that Lotus achieves ¿ 42 dB carrier cancellation gain, which translates to around 20 dB SINR lift of backscatter signal. Our field studies further show that Lotus achieves comparable throughput and communication range with other frequency-shifting based out-of-band backscatter systems yet retaining significantly higher spectrum and power efficiency.

II. Background and Motivation

A. Antenna Polarization Primer

Antenna polarization is one of the key electrical characteristics of wireless communication systems. The polarization of an antenna is loosely defined as the direction of the electromagnetic fields produced by the antenna as energy radiates away from it. These directional fields determine the direction in which the RF signal moves away from or is received by an antenna. Linear polarization and circular polarization are the most common polarization forms, as elaborated below.

• **Linear polarization**. The electric field of an antenna is confined to a single plane along the direction of propagation. When the electric field oscillates along the vertical plane, the polarization is called *Vertical Polarization (VP)*. Conversely, when the electric field oscillates along the horizontal plane, we call it *Horizontal Polarization (HP)*.

• **Circular polarization**. The radio wave rotates in a circle around the direction of propagation. A circularly polarized signal consists of two perpendicular electric fields that are equal in amplitude but have 90° difference in phase. When

[1]Specific derivation can be found in § *IV-A*.

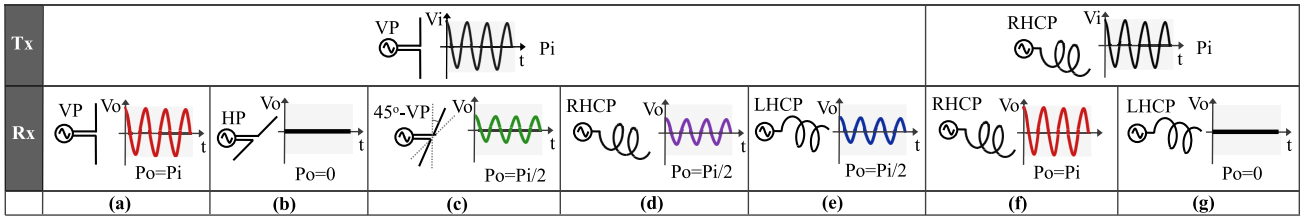

Fig. 2. Polarization mismatch between different types of transmitter antenna and receiver antenna.

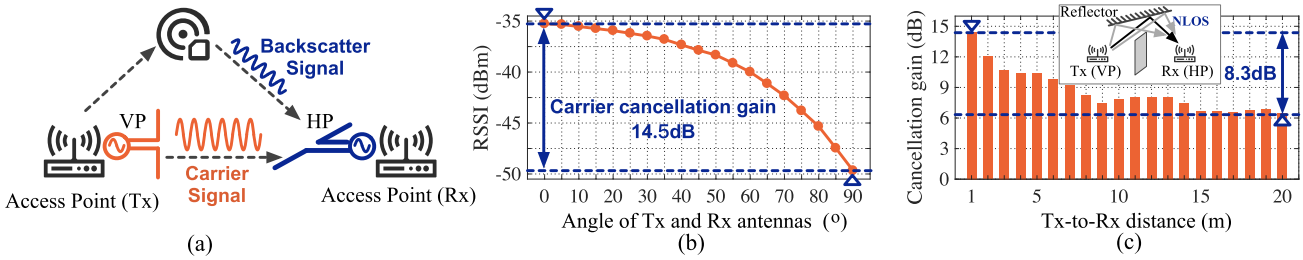

Fig. 3. Leveraging the polarization mismatch of linearly polarized antennas to cancel out the carrier signal. (a) Basic communication model. (b) The relationship between the received carrier signal strength at the Rx antenna and the polarization mismatch angle of the Rx antenna and the Tx antenna. (c) The carrier cancellation gain at different Tx-to-Rx distances.

the vertical electric field is 90° ahead of the horizontal electric field, the radio wave rotates to the right and the polarization is referred to *Right-Hand Circular Polarization (RHCP)*. When the vertical electric field is 90° behind the horizontal electric field, the radio wave rotates to the left and the polarization is referred to *Left-Hand Circular Polarization (LHCP)*.

B. Polarization Mismatch

Polarization mismatch between antennas is characterized by polarization loss factor (PLF), $0 \leq PLF \leq 1$. The more closely the two antennas are aligned in their polarization angles, the better the received signal power will be. We show six examples in Figure 2 to illustrate the polarization mismatch phenomenon and its effect on the received signal power.

(i) $PLF = 0$: when the polarization angle of the Tx antenna and Rx antenna are perfectly aligned, there will be no power loss, as shown in Figure 2(a) and Figure 2(f).

(ii) $PLF = 1$: when the polarization angle of the Tx antenna and the Rx antenna is completely mismatched, the receiver cannot receive the incident signal. For example, a horizontally polarized antenna fails to receive a signal emitted from a vertically polarized antenna, as shown in Figure 2(b). Likewise, the left-hand circularly polarized antenna fails to receive the signal emitted from a right-hand circularly polarized antenna, as shown in Figure 2(g).

(iii) $0 < PLF < 1$: the received signal strength decrease with the increasing polarization mismatch angle between the Tx and Rx antennas, as shown in Figure 2(c).

(iv) 3 dB power loss: the circularly polarized antenna can receive the signal emitted from a linearly polarized antenna with 3 dB power loss and vice versa, e.g., Figure 2(d)-(e).

C. Polarization View of Carrier Cancellation: Opportunities and Challenges

Polarization mismatch makes it difficult for the receiver to capture enough signals. This phenomenon, however, leaves an opportunity to cancel the strong carrier signal by setting the polarization of Tx and Rx antennas in a proper way.

Linear polarization mismatch. Prior works [13] (Figure 3(a)) transform the VP signal (*i.e.*, carrier signal) into an HP polarized signal (*i.e.*, backscatter signal) using a Van-atta array antenna. At the receiver, the HP Rx antenna can hardly receive the VP carrier signal due to the polarization mismatch. Instead, it can receive the HP backscatter signal. However, the carrier cancellation based on linear polarization mismatch faces multiple practical challenges when deployed in more general application scenarios.

(i) **Sensitive to the polarization mismatch angle.** The received signal strength grows rapidly with the decreasing polarization mismatch angle, as shown in Figure 3(b). To maximize the carrier cancellation, it is crucial to ensure the polarization of the Rx antenna is always in perpendicular to the polarization of the carrier generator's Tx antenna. However, this is hardly held in real-world applications such as warehouse inventory and supply chains where boxes are placed in random rotations and their positions may also change frequently.

(ii) **Limited carrier cancellation gain.** We define the carrier cancellation gain as the power loss of the carrier signal due to the polarization mismatch. Ideally, the receiver is expected to receive nothing when the Tx antenna and Rx antenna are totally mismatched. However, the optimal polarization mismatch is not achievable due to the hardware imperfection [16]. As demonstrated by Figure 3(b), we observe merely 14.5 dB carrier cancellation gain, which makes in-band backscatter decoding challenging.

(iii) **Susceptible to the reflector.** The polarization angle of the linearly polarized carrier signal may change as it bounces off the wall or other reflectors, which further complicates the polarization mismatch. To demonstrate this issue, we send a carrier signal from a VP antenna in a multi-path prevalent environment (non-line-of-sight (NLOS) scenario) and measure the received signal strength using an HP antenna. As shown in

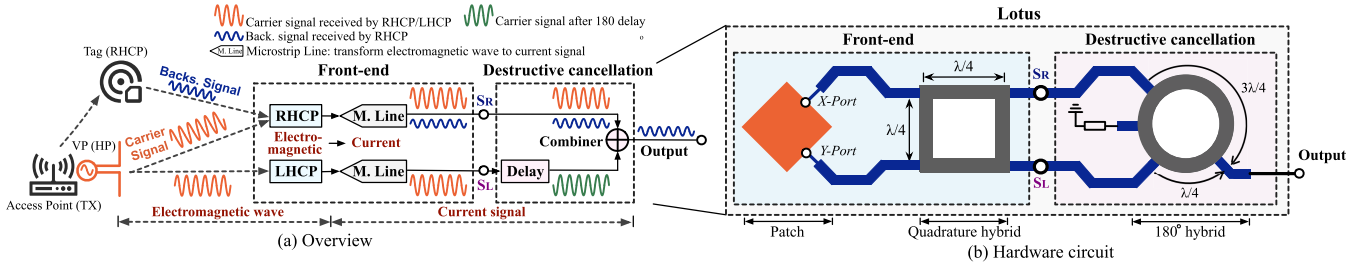

Fig. 4. Lotus design. (a) Overview. A pair of RHCP and LHCP ports are orthogonal and both can be used to receive the carrier signal. After the transmission of the microstrip line, the output signals of RHCP and LHCP ports are transformed into two identical copies of electrical signals, without polarization characteristics, but with the same amplitude, frequency, and phase. These two signals then cancel each other when we delay one path signal by half a wavelength. (b) Hardware circuit.

Figure 3(c), the carrier cancellation gain decreases by 8.3 dB as we increase the Tx-to-Rx distance. As a result, the carrier after cancellation will still be strong enough to shadow the weak backscatter signal.

III. Lotus Overview: Design Target and Solution Sketch

Basic idea. The design of Lotus is inspired by three prominent radio frequency properties, as elaborated below.

(i) Destructive interference. Two RF signals with identical frequency and amplitude but are shifted by exactly half a wavelength (*i.e.*, 180° phase offset) will add to zero.

(ii) A circularly polarized antenna (LHCP or RHCP) can receive linearly polarized (VP or HP) signals at any angle and position with 3 dB power loss (Figure 2(d)-(e)).

(iii) A left-hand circularly polarized (LHCP) antenna cannot receive the signal sent from a right-hand circularly polarized (RHCP) antenna, and vice versa, as shown in Figure 2(g).

The synergy of these three RF properties leaves us an opportunity to cancel out strong carrier signals at the analog domain without relying on sophisticated signal processing algorithms. The basic idea can be explained by Figure 4(a).

• **Cancelling carrier signals.** Without loss of generality, we assume the carrier signal comes from a linearly polarized dipole antenna. We leverage a pair of orthogonal RHCP port and LHCP port. They are orthogonal and both can be used to receive the carrier signal. After the transmission of the microstrip line, the output signals of RHCP and LHCP ports are transformed into two identical copies of electrical signals, without polarization characteristics, but with the same amplitude, frequency, and phase. Then we delay one of these two electrical copies by half a wavelength (*i.e.*, 180°) using a delay line and then add them together with an RF combiner. Since these two path signals are identical in amplitude and frequency but their phase are shifted by half a wavelength, they will cancel each other.

• **Retaining backscatter signals.** Upon detecting the carrier signal, our backscatter tag transforms the linearly polarized carrier into an RHCP backscatter signal and reflects it to the receiver. This RHCP backscatter signal will pass through only the RHCP port at the receiver and thus will survive at the RF combiner. In this way, the proposed Lotus cancels out the strong carrier while retaining the weak backscatter signal.

Figure 4(b) shows the hardware architecture of Lotus. It consists of a patch, a quadrature hybrid, plus a 180° hybrid. The carrier signal cancellation is fully implemented on the analog domain. To use it, one can simply replace the receiver antenna with Lotus to cancel out the carrier signal. We will introduce the design of Lotus in detail in the next sections.

IV. Cancelling Carrier Signals

A. RHCP and LHCP Port Construction

At first glance, the proposed carrier cancellation antenna can be realized by a pair of RHCP and LHCP antennas that are identical in their gains. In practice, however, such a solution never achieves satisfying cancellation performance because the carrier signal arrives at these two antennas along different patch paths. Hence the received signals at these two antennas will experience different attenuation loss and phase rotations. Therefore, we propose a hardware design that uses a single patch to construct a pair of RHCP and LHCP ports.

The formation principle of RHCP and LHCP. A circularly polarized signal consists of two perpendicular electric fields that are equal in amplitude but have 90° difference in phase. When the vertical electric field (S_Y) is 90° ahead of the horizontal electric field (S_X), the radio wave rotates to the right and the polarization is referred to LHCP. When the vertical electric field (S_Y) is 90° behind the horizontal electric field (S_X), the radio wave rotates to the left and the polarization is referred to RHCP.

Hardware construction. Using a single patch to construct a pair of RHCP and LHCP ports, we can ensure that these two ports can receive the same amount of energy, allowing for the reception of two identical electrical signals with the same amplitude, phase, and frequency. Figure 5 depicts the circuit design of RHCP and LHCP ports construction. The carrier signal impinges on a square patch, transferring energy to two perpendicular X-port and Y-port, respectively. We denote these two signals as S_X and S_Y. Signal S_X and S_Y then enter the quadrature hybrid from port A and port B respectively and further merge at port C and port D, respectively, as shown in Figure 5(b)-(c) ($S_X : A \rightarrow D \rightarrow C$, $S_Y : B \rightarrow C \rightarrow D$). The length of each edge of this quadrature hybrid equals to $\lambda/4$, where λ is the wavelength of the carrier signal. As the signal S_X walks $\lambda/4$ longer than signal S_Y when arriving at the port C, the phase of signal S_X would be 90° delay than that

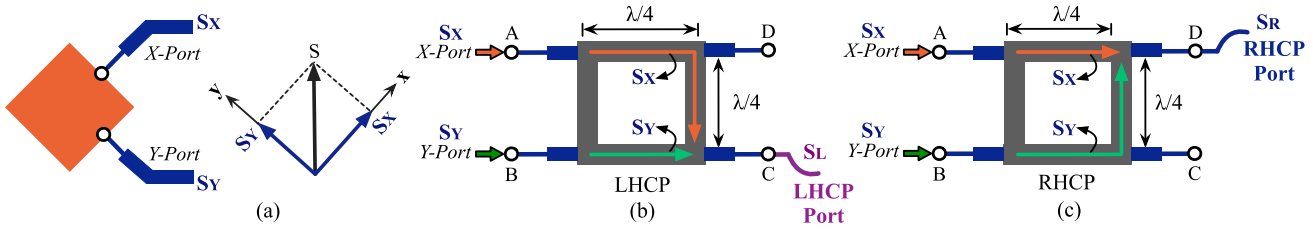

Fig. 5. Constructing a pair of RHCP and LHCP ports by using a patch plus a quadrature hybrid. (a): The incident signal impinges on a square patch, transferring energy to mutual-perpendicular $X-port$ and $Y-port$, respectively. (b): Constructing the LHCP port at port C due to the path difference of the quadrature hybrid. (c): Constructing the RHCP port at port D.

of signal S_Y. Hence we will construct a LHCP port at port C. Likewise, due to the path difference, the phase of signal S_X would be 90° advance of the phase of signal S_Y and we will get a RHCP port at port D.

Carrier signal analysis. We suppose that the incident linearly polarized carrier signal is $S = cos(\omega t)$. Two signals received by the perpendicular edges of the patch satisfy that $S_X = S_Y = \frac{\sqrt{2}}{2}cos(\omega t)$. The received signal at the LHCP port (port C) is:

$$\begin{aligned} S_L &= (S_X - \pi) + \left(S_Y - \frac{\pi}{2}\right) \\ &= \frac{\sqrt{2}}{2}cos(\omega t - \pi) + \frac{\sqrt{2}}{2}cos\left(\omega t - \frac{\pi}{2}\right) \end{aligned} \quad (1)$$

Likewise, the received signal at the RHCP port (port D) is:

$$\begin{aligned} S_R &= \left(S_X - \frac{\pi}{2}\right) + (S_Y - \pi) \\ &= \frac{\sqrt{2}}{2}cos\left(\omega t - \frac{\pi}{2}\right) + \frac{\sqrt{2}}{2}cos(\omega t - \pi) \end{aligned} \quad (2)$$

From Eq. 1 and Eq. 2, we find that $S_L = S_R$. Hence, both the RHCP port and the LHCP ports can receive the linearly polarized carrier signal. After the transmission of the microstrip line, the received signals of the RHCP and LHCP ports are transformed into two identical electric signals with the same frequency, amplitude, and phase.

In addition, the RHCP and LHCP ports suffer neither from antenna spatial diversity nor from the coupling effect, since they are built by the same front-end patch and quadrature hybrid. Figure 7 shows the frequency and radiation pattern of the LHCP port C and RHCP port D. The center frequency of both ports is well aligned with the carrier frequency at 915 MHz, as shown in Figure 7(a). They also present a similar radiation pattern in their respective main-beam (e.g., $[-90°, 90°]$), as shown in Figure 7(b). Moreover, both ports achieve 3 dBi antenna gain, as shown in Figure 7(c). These two ports also demonstrate excellent polarization properties, e.g., the axial ratio is less than 3 dB (Figure 7(d)). We also measure the signal leakage on these two parts and their impact on each other. Both $S(1,2)$ and $S(2,1)$ peak at around -40 dB on the carrier frequency band, indicating that the signal leakage from one port would not interfere the other (Figure 7(e)).

B. Destructive Combiner Cancellation

Once the linearly polarized carrier signal is received by the LHCP port and the RHCP port, it will no longer have polarization characteristics after the transmission of microstrip line.

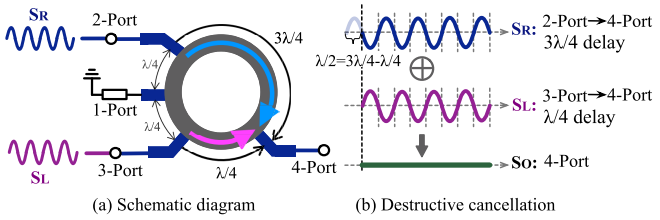

Fig. 6. Destructive combiner achieves carrier signal cancellation using a 180° hybrid.

They will be transformed into two identical electrical signals with the same frequency, amplitude, and phase. Then we send them to a 180° hybrid from two different ports, namely port 2 and port 3 as shown in Figure 6(a) ($S_R : Port2 \rightarrow Port4$, $S_L : Port3 \rightarrow Port4$). Port 2 and port 3 are the input ports while port 4 is the output port. The locations of these four ports are carefully designed to ensure the identical input signals are shifted by exactly half a wavelength when both arrive at port 4. For example, the signal S_R experience the delay of $\frac{3\lambda}{4}$ from port 2 to port 4, while the signal S_L only experience the delay of $\frac{\lambda}{4}$ from port 3 to port 4. Accordingly, these two path signals will add destructively at port 4:

$$S_O = \left(S_R + \frac{3\pi}{2}\right) + \left(S_L + \frac{\pi}{2}\right) = S_R - S_L = 0 \quad (3)$$

Hence, the received carrier signals by RHCP and LHCP ports cancel each other completely.

V. Retaining Backscatter Signals

A. Tag Antenna Selection

The backscatter tag modulates data on top of the linearly polarized carrier signal and reflects it to the receiver. To survive at the Lotus, the backscatter signal should be circularly polarized. Directly, we can use a a single-port RHCP antenna for both carrier reception and backscatter reflection. The RHCP antenna can receive the linearly polarized carrier signal with 3 dB loss and transform it into a circularly polarized backscatter signal, as illustrated in Figure 2(d). In order to compensate for the power loss caused by the mismatch between the LP and the tag's antenna, we leverage the tunnel diode to amplify the backscatter signal

Backscatter signal analysis. The backscatter signal reflected from the tag with the RHCP antenna can be represented as $S = \frac{\sqrt{2}}{2}\vec{e_x}\,cos(\omega t) + \frac{\sqrt{2}}{2}\vec{e_y}\,cos\left(\omega t + \frac{\pi}{2}\right)$. Retrospect

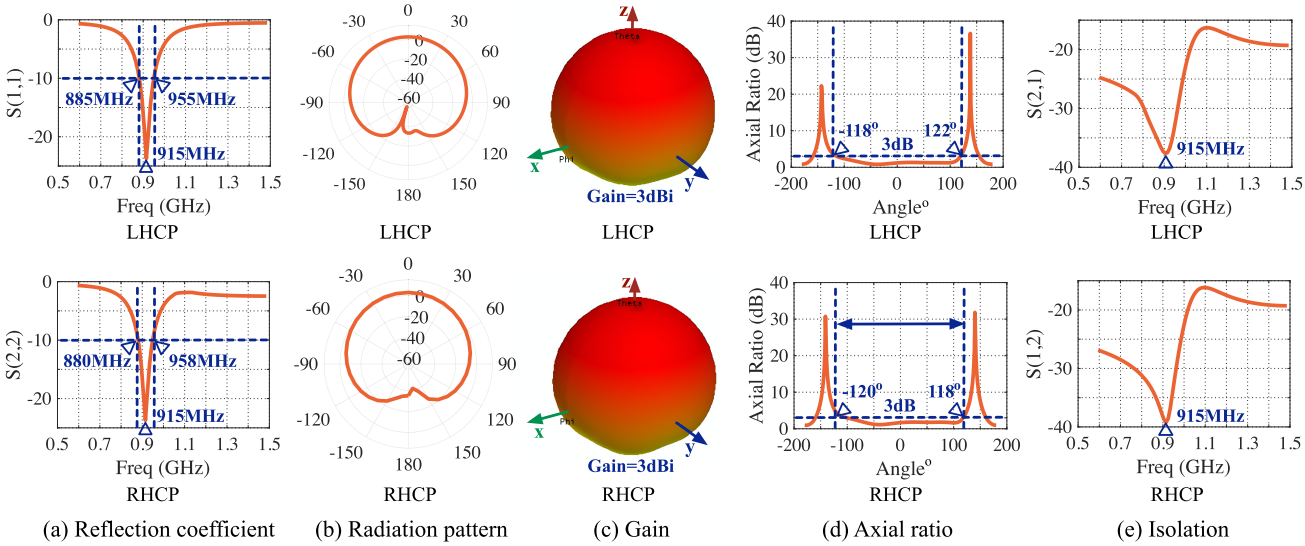

Fig. 7. Characterizing the performance of Lotus antenna. (a): The reflection coefficient of each port. (b): The radiation pattern of each port. (c): The antenna gain of each port. (d): The axial ratio of each port. (e): The isolation between two ports.

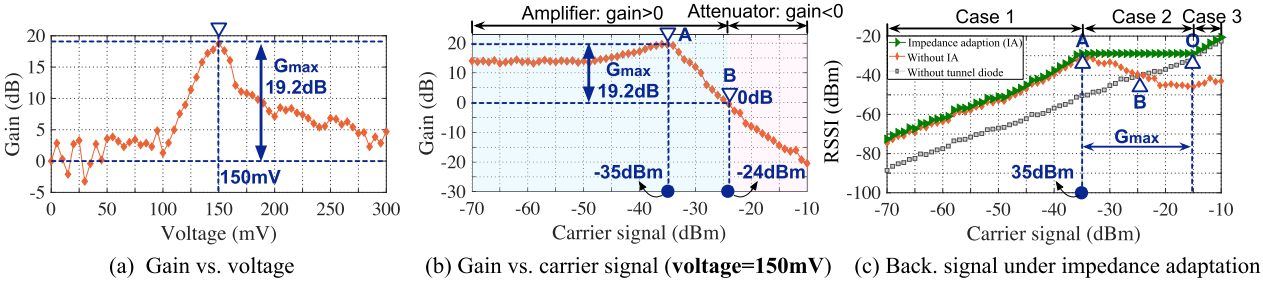

Fig. 8. Illustration of the amplification gain of the tunnel diode. (a): The amplification gain of the tunnel diode changes with its bias voltage. (b): The amplification gain is also affected by the incident signal strength. The amplification gain drops when the incident signal strength is higher than −35 dBm. The tunnel diode further turns into an attenuator when the incident signal strength exceeds −24 dBm. (c): Comparison of backscatter signal strength in the presence/absence of the impedance adaptation and tunnel diode.

to Figure 5, two signals received by the perpendicular edges of the patch satisfy that $S_X = \frac{\sqrt{2}}{2}cos(\omega t)$ and $S_Y = \frac{\sqrt{2}}{2}cos\left(\omega t + \frac{\pi}{2}\right)$. Then the received signal at the LHCP port (port C) is:

$$S_L = (S_X - \pi) + \left(S_Y - \frac{\pi}{2}\right) = \frac{\sqrt{2}}{2}cos(\omega t - \pi) + \frac{\sqrt{2}}{2}cos(\omega t) = 0 \quad (4)$$

The received signal at the RHCP port (port D) is:

$$\begin{aligned} S_R &= \left(S_X - \frac{\pi}{2}\right) + (S_Y - \pi) \\ &= \frac{\sqrt{2}}{2}cos\left(\omega t - \frac{\pi}{2}\right) + \frac{\sqrt{2}}{2}cos\left(\omega t + \frac{\pi}{2} - \pi\right) \\ &= \sqrt{2}cos\left(\omega t - \frac{\pi}{2}\right) \end{aligned} \quad (5)$$

Hence, the backscatter signal only passes through the RHCP port and thus survives at the destructive combiner.

B. Backscatter Signal Amplification

Tunnel diode primer. Tunnel diode features a unique *negative resistance* property where an increase in voltage across the diode's terminals results in a decrease in electric current through it [14]. While a positive resistance consumes power from current passing through it, a negative resistance produces power, making tunnel diode a low-power power amplifier with only a few tens of milliwatts.

The pitfall in using tunnel diode as an amplifier. However, adopting a tunnel diode as a backscatter signal amplifier faces a fundamental challenge: *amplification gain drift*. In particular, the amplification gain of a tunnel diode is not only determined by its bias voltage (Figure 8(a)) but also affected by the incident signal because the RF power will change the impedance of the tunnel diode. Figure 8(b) shows the amplification gain of the tunnel diode AI301A in different incident signal strength settings. The amplification gain grows first and then drops rapidly with the growing incident signal power. For instance, when the incident signal strength grows from −35 dBm to −24 dBm, the amplification gain drops from 19.2 dB to 0 dB. As the incident signal strength grows further, the tunnel diode then turns into an attenuator, introducing up to 22 dB power attenuation to the incident signal.

Maximize the backscatter signal strength by impedance adaptation. To address the above challenge, we propose an online impedance adaptation mechanism to ensure the

tunnel diode never turns into an attenuator. Different from conventional impedance matching networks [17] where the impedance is tuned to maximize the portion of incident signal power that can be transformed into electric signals, our proposed solution tunes the matching network so that the transformed electric signal power always leads to the maximum backscatter signal strength. Taking into account both amplification gain and incident signal strength, we propose an impedance adaption algorithm as elaborated below. Without loss of generality, we denote the incident carrier signal power and the maximum amplification gain of the tunnel diode as P and G_{max}, respectively. For the tunnel diode used by our system, $G_{max} = 19.2$ dB (Figure 8(a) and Figure 8(b)). We introduce three strategies for the following thress cases.

• **Case One:** P **‘! −35 dBm**. As shown in Figure 8(b), when the incident carrier signal strength is lower than -35 dBm, the amplification gain of the tunnel diode grows with the increase of the carrier signal strength. Following the conventional impedance-matching design, we tune the impedance-matching network of the backscatter tag to ensure most of the carrier signal power can be absorbed by the antenna.

• **Case Two: −35 dBm** $\leq P \leq -35$ **dBm** $+G_{max}$ ($G_{max} = 19.2$ dB). When the incident carrier signal strength is higher than -35 dBm but lower than -35 dBm $+G_{max}$, the amplification gain of the tunnel diode drops. In this case, we intentionally tune the impedance-matching network into an unmatched state so that only part of its power (*i.e.*, -35dBm) is transformed into electric signals. In this way, the tunnel diode will stay in the amplifier state with the maximum amplification gain.

• **Case Three:** P **¿ −35 dBm** $+G_{max}$ ($G_{max} = 19.2$ dB). When the carrier signal is even stronger, exceeding -35 dBm $+G_{max}$, to retain the maximum amplification gain of the tunnel diode, the backscatter tag has to reduce the incident signal power by P - (-35) dBm–a value higher than the maximum amplification gain G_{max} that this tunnel diode can bring to the backscatter signal. In this case, the use of a tunnel diode will not help the signal amplification. We turn off the tunnel diode on the backscatter tag in this case.

Considering both the incident signal strength and the amplification gain of the tunnel diode, Figure 8(c) compares the backscatter signal strength before (line in orange) and after (line in green) impedance adaptation in different incident signal strength settings. We also show the backscatter signal strength without using the tunnel diode (the line in gray) for comparison. Evidently, the backscatter signal strength with impedance adaptation is always equal or higher than the other two cases across all incident carrier signal strength settings.

Extending to other types of tunnel diodes. In practice, both G_{max} and the inflection point (point A in Figure 8(c)) would change with the types of the tunnel diode. One can obtain these parameters offline and hardcode them into the tag's microcontroller.

Practical system workflow. Figure 9 shows the circuit schematic of this backscatter tag design. The tag detects the incident carrier signal and measures its power with a passive envelope detector. We use the HSMS-286x series surface mount microwave Schottky diode to build the envelope

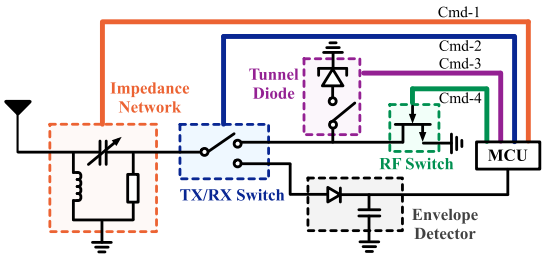

Fig. 9. The circuit schematic of backscatter tag.

detector. It can achieve a sensitivity of -57 dBm with low power consumption. Then the MCU selects different reflection modes based on the measured incident signal strength. For case one where the carrier signal is relatively weak, the computing unit enables the tunnel diode and the RF switch by signaling a `Cmd-3` and a `Cmd-4` command respectively. The Tx switch is also turned on by a `Cmd-2` signal. For case two, the computing unit tunes the capacitance of a variable capacitor connected to the load impedance matching network by signaling a `Cmd-1` command. The higher the capacitance, the more significant the mismatch between the load impedance and the source impedance (*i.e.*, 50 Ω), and so does the higher power loss of the incident signal. The backscatter tag tunes this variable capacitor in a step of 0.1 pF until the detected carrier signal strength drops to -35 dBm. The time overhead of our impedance adjustment algorithm is proportional to the difference between the incident carrier strength and the desired carrier strength corresponding to the maximum backscatter signal strength. Our empirical experiments show that the time overhead of our impedance adjustment algorithm is within 2.5 seconds. For case three, the computing unit disables the tunnel diode with a signal `Cmd-3` while keeping both the RF switch and the Tx switch open.

C. Overall SINR Improvement Analysis

The SINR improvement stems from two parts: i): carrier cancellation gain brought by the Lotus antenna; and ii): the power gain of backscatter signal brought by the tunnel diode. These gains enable Lotus to achieve comparable performance with other out-of-band backscatter systems of frequency-shifting technique. We ablate these two parts and the ablation study can be found in § VII-B.

D. Power Consumption Analysis

The variable capacitor. In our design, we use the variable components TZB4Z, TZB4R, and TZB4P series (the voltage-controlled capacitor LXRW0YV600-054) to adjust the impedance matching network. When the bias voltage changes from 0 V to 3 V, the capacitance of LXRW0YV600-054 varies from 60 pF to 30 pF, and it can support the working frequency of 1 MHz. The power consumption of the variable capacitor is about 135 μW at the μW-level.

ADC sampling. We utilize the built-in ADC on the MSP430 for sampling. When the ADC is in idle mode, its current is only 0.3 μA. When the ADC is in active mode (i.e., when it

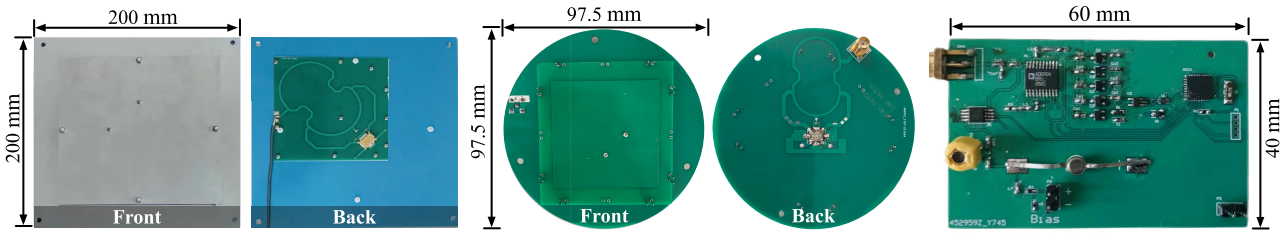

(a) Lotus antenna at the receiver (915MHz) (b) Lotus antenna at the receiver (2.4GHz) (c) Backscatter tag

Fig. 10. Lotus antenna and backscatter tag prototypes.

is sampling analog signals), the current is low and usually ranges from 25 μA to 1.2 mA (@3 V), corresponding to sampling rates of 1 Ksps to 200 Ksps. In our design, the energy consumption of ADC is 255 μW when adopting the sampling rate of 10 Kbps.

E. Operation Context

Continuous Carrier Excitation. Lotus operates under a continuous-wave (CW) carrier excitation context, such as a persistent sinusoidal tone from a dedicated transmitter or ambient source like stable LoRa chirp signals. This excitation is not transient frame-based. The carrier signal is present for extended periods (seconds/minutes/hours) during normal operation scenarios, such as inventory scanning and sensor monitoring. Given a continuous and stable carrier excitation, an impedance adjustment time of 2.5 s is acceptable.

Event-driven Adjustment. The impedance network adopts an event-driven adjustment. The impedance adjustment usually occurs once during initialization or significant incident power changes (e.g., tag movement relative to the carrier source). Once calibrated, the tunnel diode maintains stable amplification for a fixed Tx-tag distance. Therefore, the impedance matching adjustments will not occur frequently. The tag reflects the backscatter data uninterruptedly during the stable state. Our experiment results also demonstrate the sustained SINR gains over hours without recalibration.

VI. Implementation

Lotus antenna at the receiver. We design Lotus antenna using ANSYS HFSS software and fabricate two prototypes working on 915 MHz and 2.4 GHz ISM bands respectively using the aluminum alloy material with 8.5 mm thickness, as shown in Figure 10(a)–(b). Our Lotus antenna is completely passive and its material cost is less than 5 USD.

Lotus tag. We prototype Lotus tag on a 60 mm $\times$40 mm one-layer Printed Circuit Board (PCB) using commercial off-the-shelf circuit components and a low power MSP430 [18] MCU. We equip Lotus tag with a commercial omnidirectional RHCP antenna [19] with 3 dBi gain. The tag consists of five major components: impedance network, envelope detector, tunnel diode, RF switch, and MSP430 controller. Figure 10(c) shows its PCB implementation. We use a palm-size solar panel to power the tag.

Transmitter and receiver. We use two software-defined radios USRP N210 as transmitter and receiver. The transmitter

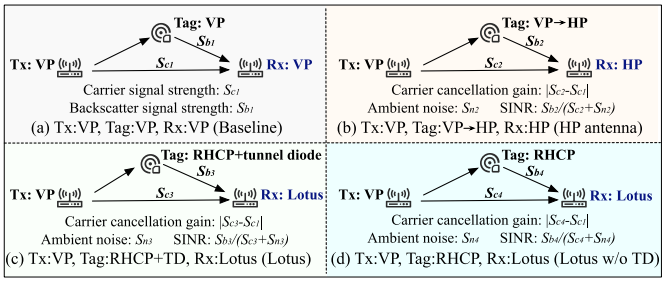

Fig. 11. Evaluation setting and metric calculation.

send out a continuous sinusoidal tone as the carrier signal through an omnidirectional, vertically polarized antenna with 3 dBi gain [20]. The transmission power is set to 20 dBm. The receiver equipped with the Lotus antenna of 3 dBi gain runs open-sourced gr-lora [21], gr-bluetooth [22], and gr-ieee802-11 [23] to decode the backscattered LoRa, Bluetooth, and WiFi.

Plug-and-play. Lotus antenna is an entirely passive peripheral. To cancel out the carrier interference, one can simply replace the default antenna on the receiver with Lotus antenna with neither software upgrading nor hardware modification to the receiver radio chains. On the other hand, we can easily integrate Lotus front-end into existing backscatter tag designs with ignorable engineering efforts. To demonstrate this point, we integrate Lotus front-end into a programmable backscatter radio design named RF-Transformer [24] and test Lotus's performance in various backscatter technologies including Wi-Fi, Zigbee, and LoRa. Specifically, we replace its impedance matching module with our impedance adaptation networks and add the tunnel diode to its RF switch while retaining all the remaining functional units unchanged. This radio front-end design allows the backscatter tag to remedy the 3 dB loss due to the mismatch of the linearly polarized carrier signal and the circularly-polarized antenna with around 70 μW extra power consumption.

VII. Evaluation

Metric. We adopt four metrics to assess Lotus's performance. The metric calculation is shown in Figure 11.

(1) Carrier cancellation gain: we measure the received carrier signal at the receiver twice. The first measurement is taken in a linearly aligned state (Tx: VP, Rx: VP) and we take this measurement as the baseline shown in Figure 11(a). The second measurement is taken in a linearly mismatched

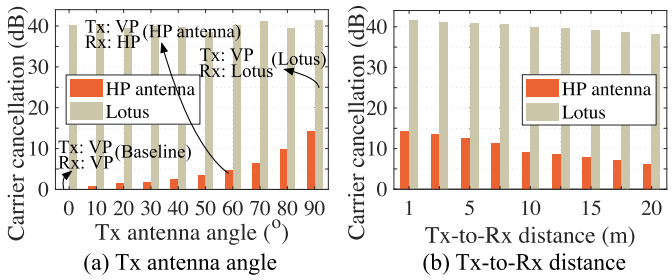

Fig. 12. Comparison of the carrier cancellation gain brought by the VP antenna (Figure 11(a)), HP antenna (Figure 11(b)), and Lotus (Figure 11(c)).

state (Tx: VP, Rx: HP) and in the presence of Lotus (Tx: VP, Rx: Lotus), as shown in Figure 11(b-d). The difference in the signal strength between these two carrier signal measurements is defined as carrier cancellation gain.

(2) SINR refers to the power ratio of the backscatter signal to the carrier signal plus the noise.

A. Carrier Cancellation Gain

1) Comparison With Linear Polarization Mismatch: **Impact of Tx antenna's polarization angle**. As shown in Figure 11(b) and Figure 11(c), we place the transmitter 1 m away from the receiver. The transmitter antenna then spins from 0° (HP) to 90° (VP). For comparison, we place an HP antenna and Lotus antenna on the receiver, then measure the carrier cancellation. The result is shown in Figure 12(a), we observe that the carrier cancellation gain of the HP receiver antenna varies dramatically with the variation of the Tx antenna's polarization angle. The carrier cancellation gain grows from around 0 dB to 14.2 dB when it is fully misaligned with the transmitter antenna. On the contrary, Lotus antenna achieves consistently high (38.6 dB–41.5 dB) gain across all Tx antenna's polarization angle settings. This is expected since our circularly polarized design is immune to the angle variation of the transmitter antenna.

Impact of Tx-to-Rx distance. We then measure the carrier cancellation gain in different Tx-to-Rx distance settings. The longer the Tx-to-Rx distance, the more severe the multi-path effect would be. As shown in Figure 12(b), when the Tx-to-Rx distance grows from 1 m to 20 m, the carrier cancellation gain of the HP receiver antenna drops by 2.3× (*i.e.*, from 14.2 dB to 6.2 dB). In contrast, the carrier cancellation gain of Lotus antenna only drops slightly from 41.5 dB to 38.2 dB. These results demonstrate that the linearly polarized mismatch design is susceptible to multi-path effect whereas Lotus antenna is not. The carrier cancellation gain of Lotus antenna is 27.3 dB–32 dB (2.9×–6.2×) higher than that of the HP antenna across all Tx-to-Rx distances.

2) Micro-Benchmarks: **Impact of signal bandwidth.** We place the transmitter 1 m away from the receiver. The Tx transmits a sine wave (as the carrier) at a central frequency of 915 MHz. We then vary the bandwidth of this sine wave from 125 KHz to 20 MHz. The result is shown in Figure 13(a). Lotus antenna achieves a consistently high carrier cancellation gain at around 38.5 dB–42.7 dB when the bandwidth is below 2 MHz. The carrier cancellation gain then drops from 38.5 dB to 27.6 dB with increasing signal bandwidth. This is expected since the effective bandwidth of the antenna is usually limited.

Impact of the center frequency. We repeat the above experiment on the 2.4 GHz band and show the results in Figure 13(b). Although the averaged carrier cancellation gain drops slightly with increasing signal bandwidth, it is still above 36.5 dB when the bandwidth grows to 20 MHz at 2.4 GHz. Compared with the 915 MHz band, Lotus antenna at 2.4 GHz achieves a higher carrier cancellation gain at a larger bandwidth. For instance, the carrier cancellation gain at 2.4 GHz is 1.3× higher than that at 915 MHz when the bandwidth of carrier signals both are 20 MHz. This is expected since the effective bandwidth of the RHCP and LHCP ports of Lotus antenna scales with the center frequency.

Impact of different modulation schemes. We measure the carrier cancellation gain at different carrier signal modulation settings. As shown in Figure 13(c), the Lotus antenna achieves a consistently high carrier cancellation gain for all three types of modulated signals, including sine signals (42.4 dB), BPSK signals (40.2 dB), and FSK signal (38.6 dB). The carrier cancellation gain gradually drops to 33.9 dB and 32.6 dB for the chirp-modulated signals and OFDM symbols.

B. SINR Improvement

The SINR improvement stems from two parts: carrier cancellation gain brought by the Lotus antenna; and the amplification gain of backscatter signal brought by the tunnel diode. We measure the SINR improvement by ablating these two parts. The experimental setting is shown in Figure 11. The transmitter adopts a VP antenna with 3 dBi antenna gain. The receiver[2] is equipped with the VP antenna (Figure 11(a), baseline), HP antenna (Figure 11(b), baseline), Lotus with tunnel diode (Figure 11(c)), and Lotus without tunnel diode (Figure 11(d)) to receive the backscatter signal. In this experiment, we put the tag 1 m away from the transmitter and then gradually increase the distance between the transmitter and the receiver (Tx-to-Rx distance). We measure the SINR of the backscatter signal at the receiver in each distance setting.

SINR improvement from the Lotus antenna. Figure 13(d) shows the evaluation result and we find that the SINR of all four designs declines with the increase of the Tx-to-Rx distance. This is expected because the backscatter signal attenuates with increasing link distance. Nevertheless, compared with the VP antenna (Figure 11(a)) and HP antenna (Figure 11(b)), our Lotus antenna Figure 11(c) still improves the SINR by 33.1 dB–35.2 dB and 20.4 dB–25.8 dB respectively across different distances.

SINR improvement from the tunnel diode. We measure the SINR of the backscatter signal at the receiver with and without the tunnel diode, respectively. Figure 13(d) shows the result. We observe that the tunnel diode brings about 18.7 dB –11.2 dB gain (*i.e.*, the gap between the purple line and blue line) to the SINR of the backscatter signal consistently.

Impact of adaptive impedance network. We further assess the effectiveness of the adaptive impedance network. The

[2]These antennas (VP, HP, and Lotus) at the Rx have the same gain of 3 dBi.

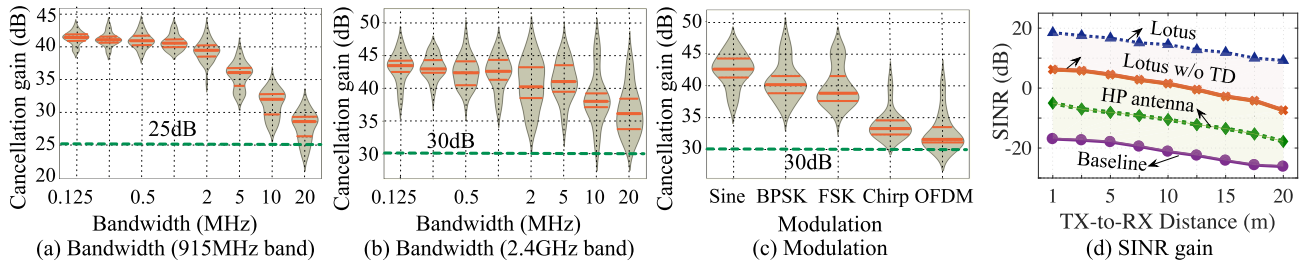

Fig. 13. (a)–(c): Carrier cancellation gain under different bandwidth (900MHz and 2.4GHz) and modulation scheme settings. The evaluation setting is shown in Figure 11(c). (d): SINR gain under different Tx-to-Rx distance settings. The evaluation setting is shown in Figure 11(a)–(d).

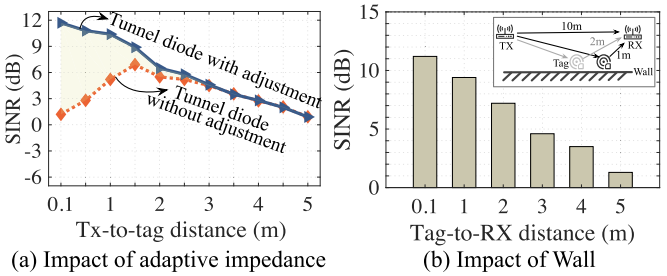

Fig. 14. SINR benchmark. (a): Impact of adaptive impedance. (b): Impact of the wall.

result is shown in Figure 14(a). The SINR without adaptive impedance network grows first and then drops with the Tx-to-tag distance, because the strong carrier strength negatively affects the amplification gain of the tunnel diode, as explained in Figure 8(c). We observe that the adaptive impedance network achieves a higher SINR of the backscatter signal (up to 10.5 dB higher than that without the adaptive impedance network) when the tag is close to the carrier generator (*i.e.*, $<$ 3 m).

Impact of the wall. Next, we access Lotus performance under the impact of the wall. We place the tag in front of a wall and then change the tag-to-Rx distance to measure the SINR at the receiver. The result is shown in Figure 14(b). We observe the SINR drops by 9.6 dB from 11.2 dB to 1.6 dB when the Tag-to-Rx distance varies from 0.1 m to 5 m. Compared with the results in the open scenarios, the performance of Lotus deteriorates in front of the walls.

C. Field Studies

Backscatter distance and throughput. As shown in Figure 15(a) and Figure 15(b), the performance of Lotus is comparable to that of the frequency-shifting-based design. The backscatter distance of Lotus is 1.08× (425 m vs. 460 m), 1.06× (23.2 m vs. 24.6 m), and 1.16× (24.6 m vs. 21.2 m) shorter than that of the frequency-shifting-based design for the LoRa, Bluetooth, and Wi-Fi 802.11b backscatter links. The throughput of Lotus is 1.04× (1.88 Kbps vs. 1.94 Kbps),1.05× (116.4 Kbps vs. 122.2 Kbps), and 1.08× (244.6 Kbps vs. 227.2 Kbps) lower than that of the frequency-shifting-based design for the LoRa, Bluetooth, and Wi-Fi 802.11b backscatter links. In addition, the carrier cancellation gain of Lotus antenna declines with the increase of signal bandwidth (*c.f.* Figure 12(d)). Hence we expect inferior cancellation gain of Lotus for Wi-Fi 802.11b signals where the link bandwidth is 20 MHz.

Spectrum and power efficiency. We compare the spectrum and power efficiency of Lotus and the frequency-shifting based interference avoidance design. Lotus achieves 3.88 bit/KHz, 115.6 bit/KHz, and 11.8 bit/KHz spectrum utilization on LoRa, Bluetooth, and Wi-Fi 802.11b backsscatter, which is 2.02×, 1.89×, and 1.9× higher than the baseline (Figure 15(c)). Likewise, the power efficiency of Lotus is 6.71× (7.18 bit/uJ vs. 1.07 bit/uJ), 6.52× (374.53 bit/uJ vs. 57.47 bit/uJ), and 5.1× (86.1 bit/uJ vs. 17.2 bit/uJ) higher than that of the tag with frequency shifting for the LoRa, Bluetooth, and Wi-Fi 802.11b backscatter links (Figure 15(d)).

VIII. Related Work

Backscatter radio has emerged as a promising communication solution for the development of IoT [25], [26], [27], [28], [29]. We review related works and highlight our difference.

Carrier interference avoidance. Frequency shifting [10], [11], [30], [31], [32], [33], [34], [35], [36] moves weak backscatter signals to a non-overlapping frequency band to avoid carrier interference. For instance, FS-Backscatter [10] shifts the carrier signal by 20 MHz to backscatter Wi-Fi and Bluetooth signals. PLoRa [11] takes ambient LoRa transmissions as the excitation signals and modulates the original LoRa chirp signal into a new standard LoRa chirp signal at another frequency band. SHIFT [33] generates the frequency shifting signals by using twin carrier tones on different frequency bands. Although these systems can successfully avoid strong interference from the carrier signal, they are often not spectrum efficient and would inevitably crowd the wireless spectrum on the ISM band. Generating tens of MHz oscillating signals is power-intensive that burdens the power budget of the tag.

Carrier interference cancellation. Another trail of efforts adopts interference cancellation techniques to mitigate the carrier interference [4], [5], [6], [7], [8], [37]. Turbocharging [37] uses the multi-antenna receiver with the coding mechanism to cancel the carrier signals, but it is only suitable for the envelope detector type of receiver. Other works develop full-duplex radios to reduce interference. Reference [7] presents an analog cancellation circuit to realize a full duplex Wi-Fi radio. BackFi [4] takes advantage of the above design to suppress carrier interference in Wi-Fi backscatter systems.

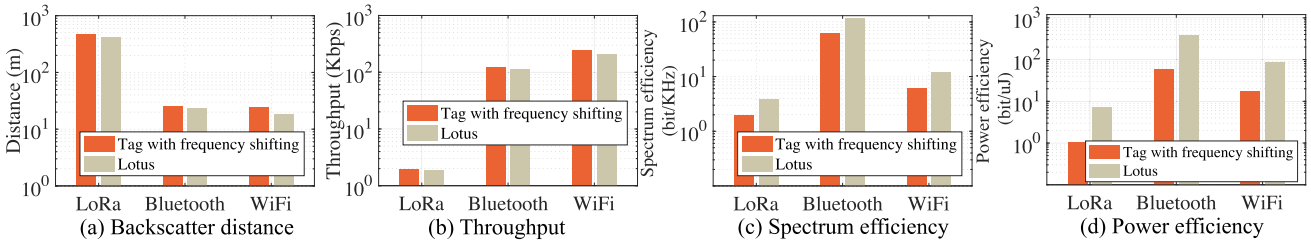

Fig. 15. Performance of LoRa, Bluetooth and Wi-Fi backscatter links in the presence of Lotus.

Reference [5] builds a full-duplex LoRa backscatter reader using a hybrid-coupler architecture for strong interference cancellation. Reference [8] proposes a wideband full-duplex wireless design via frequency domain equalization. However, most of these designs are dedicated, bulky, and expensive, requiring complex hardware circuits and software estimation algorithms, which sets a strong barrier to their ubiquitous adoption.

Antenna polarization. As an orthogonal thread, recent works [13], [38], [39], [40], [41] explore antenna polarization to deal with carrier interference. Reference [38] evaluates the performance of polarization mismatch on the drone systems. The authors in [41] propose a polarization-based reconfigurable antenna that can switch between several polarization angles to improve the robustness against carrier interference. Reference [39] leverages the antenna polarization for interference cancellation in full-duplex radios. mmTag [13] adopts perpendicular antennas at the transmitter and the receiver with orthogonal polarization angle so that the receiver antenna can hardly receive the strong carrier signal in millimeter-wave backscatter networks.

Impedance matching. Impedance matching aims to adjust the signal reflection/absorption by manipulating the source and load impedance [42] based on Smith chart [24]. Likewise, our system tunes the matching network based on the Smith chart so that the transformed electric signal power always leads to the maximum amplification gain of the tunnel diode.

Difference with existing designs. Compared to the interference avoidance solutions, Lotus is power efficient and spectrum efficient. Compared to the interference cancellation methods, Lotus costs significantly less and can be rapidly deployed on existing receivers. Compared to antenna polarization-based solutions, Lotus is resilient to multi-path effect and has no requirement on the placement of transmitter and tag.

IX. Discussion

Applicability issue and impact of multi-path. Lotus is optimized to cancel linearly polarized (LP) carrier signals, and the requirement of an LP carrier generator limits its applicability since many wireless systems use CP or MIFA antennas. However, Lotus still offers significant value in applications where LP interference is a primary concern. For example: (1) RFID and IoT Networks. Most low-cost IoT devices adopted one cheap, linearly polarized dipole antenna. RFID readers in warehouses or factories face interference from nearby devices. Lotus can enhance read accuracy by canceling overlapping LP carrier noise. (2) Wi-Fi and cellular networks. LP antennas are common in Wi-Fi routers and base stations. Lotus can reduce cross-inteference from the nearby devices in high-density environments such as stadiums and offices. (3) Terrestrial microwave links. Point-to-point microwave systems (e.g., 5G backhaul) often employ LP antennas. Lotus can suppress co-channel LP interference in dense urban deployments, improving link reliability. In addition, we admit that Lotus has some limitations. For instance, in scenarios where signal polarization shifts due to reflections (e.g., multi-path), Lotus's efficacy may degrade unless paired with adaptive polarization-tracking systems.

Impact of orientation. The proper alignment of the Lotus antenna is critical for optimal performance. If the antenna is rotated, the X and Y component magnitudes of the received signal will no longer remain equal, leading to an imbalance in the detected RHCP and LHCP signal strengths. In this way, the circularly polarized (CP) signals (RHCP/LHCP), which inherently require equal X/Y magnitudes and a 90° phase difference, will be converted into the elliptically polarized signals. As a result, Lotus cannot fully suppress the residual elliptical components, leading to degraded carrier cancellation.

Impact of bandwidth and frequency band. The carrier cancellation gain of Lotus drops with the increase of bandwidth. This is expected since the effective bandwidth of the antenna is usually limited. The larger the bandwidth, the more severe the signal loss and leakage. Lotus antenna achieves a consistently high carrier cancellation gain at around 38.5 dB–42.7 dB when the bandwidth is below 2 MHz. The carrier cancellation gain then drops from 38.5 dB to 27.6 dB with increasing signal bandwidth. In addition, Lotus can achieve good performance across the frequency bands from 900 MHz to 2.4 GHz. This is because the principle of carrier cancellation is applicable in different frequency bands. Compared with the 915 MHz band, Lotus antenna at 2.4 GHz achieves a higher carrier cancellation gain at a larger bandwidth. For instance, the carrier cancellation gain at 2.4 GHz is 1.3X higher than that at 915 MHz when the bandwidth of carrier signals both are 20 MHz. This is expected since the effective bandwidth of the RHCP and LHCP ports of Lotus antenna scales with the center frequency.

X. Conclusion

We have presented the design, implementation, and evaluation of Lotus, a plug-and-play hardware solution for carrier cancellation in backscatter communication systems. Lotus antenna replaces the receiver's default antenna to cancel out

the carrier interference, with neither software modification nor hardware upgrading to receiver's radio chains. The evaluation shows that Lotus achieves 42 dB carrier cancellation gain, which translates to around 20 dB SINR lift of backscatter signal. Lotus also achieves comparable throughput and communication range with other out-of-band backscatter systems.

REFERENCES

[1] X. Guo et al., "Aloba: Rethinking ON-OFF keying modulation for ambient LoRa backscatter," in *Proc. ACM SenSys*, 2020, pp. 192–204.

[2] X. Guo et al., "Saiyan: Design and implementation of a low-power demodulator for LoRa backscatter systems," in *Proc. USENIX NSDI*, Renton, WA, USA, 2022, pp. 437–451.

[3] P. Hu, P. Zhang, and D. Ganesan, "Laissez-faire: Fully asymmetric backscatter communication," in *Proc. ACM SIGCOMM*, 2015, pp. 255–267.

[4] D. Bharadia, K. R. Joshi, M. Kotaru, and S. Katti, "BackFi: High throughput WiFi backscatter," in *Proc. ACM Conf. Special Interest Group Data Commun.*, Budapest, Hungary, Aug. 2015, pp. 283–296.

[5] M. Katanbaf, A. Weinand, and V. Talla, "Simplifying backscatter deployment: Full-duplex LoRa backscatter," in *Proc. USENIX NSDI*, Apr. 2020, pp. 955–972.

[6] V. Liu, V. Talla, and S. Gollakota, "Enabling instantaneous feedback with full-duplex backscatter," in *Proc. 20th Annu. Int. Conf. Mobile Comput. Netw.*, Sep. 2014, pp. 67–78.

[7] D. Bharadia, E. McMilin, and S. Katti, "Full duplex radios," in *Proc. ACM SIGCOMM Conf. SIGCOMM*, Aug. 2013, pp. 375–386.

[8] T. Chen, M. Baraani Dastjerdi, J. Zhou, H. Krishnaswamy, and G. Zussman, "Wideband full-duplex wireless via frequency-domain equalization: Design and experimentation," in *Proc. 25th Annu. Int. Conf. Mobile Comput. Netw.*, Los Cabos, Mexico, Aug. 2019, pp. 1–16.

[9] M. Bansal, A. Schulman, and S. Katti, "Atomix: A framework fo deploying signal processing applications on wireless infrastructure," in *Proc. USENIX NDSI*, 2015, pp. 173–188.

[10] P. Zhang, M. Rostami, P. Hu, and D. Ganesan, "Enabling practical backscatter communication for on-body sensors," in *Proc. ACM SIGCOMM Conf.*, Salvador, Brazil, Aug. 2016, pp. 370–383.

[11] Y. Peng et al., "PLoRa: A passive long-range data network from ambient LoRa transmissions," in *Proc. Conf. ACM Special Interest Group Data Commun.*, Aug. 2018, pp. 147–160.

[12] X. Na, X. Guo, Z. Yu, J. Zhang, Y. He, and Y. Liu, "Leggiero: Analog WiFi backscatter with payload transparency," in *Proc. 21st Annu. Int. Conf. Mobile Syst., Appl. Services*, Helsinki, Finland, Jun. 2023, pp. 436–449.

[13] M. H. Mazaheri, A. Chen, and O. Abari, "MmTag: A millimeter wave backscatter network," in *Proc. ACM SIGCOMM Conf.*, Aug. 2021, pp. 463–474.

[14] A. Varshney, A. Soleiman, and T. Voigt, "TunnelScatter: Low power communication for sensor tags using tunnel diodes," in *Proc. 25th Annu. Int. Conf. Mobile Comput. Netw.*, Oct. 2019, pp. 1–17.

[15] X. Guo, B. Liu, N. Jing, C. Gu, Y. Shu, and J. Chen, "Enabling cross-band backscatter communication with twaltz," *IEEE Trans. Mobile Comput.*, vol. 24, no. 11, pp. 11323–11336, Nov. 2025.

[16] L. Chen, W. Hu, K. Jamieson, X. Chen, D. Fang, and J. Gummeson, "Pushing the physical limits of IoT devices with programmable metasurfaces," in *Proc. USENIX NSDI*, Apr. 2020, pp. 425–438.

[17] M. R. Abdelhamid, R. Chen, J. Cho, A. P. Chandrakasan, and F. Adib, "Self-reconfigurable micro-implants for cross-tissue wireless and batteryless connectivity," in *Proc. 26th Annu. Int. Conf. Mobile Comput. Netw.*, Sep. 2020, pp. 1–14.

[18] *Microcontroller MSP430*. Accessed: Sep. 1, 2024. [Online]. Available: https://www.ti.com/microcontrollers-mcus-processors/msp430-microcontrollers/overview.html

[19] *Omnidirectional RHCP Antenna*. Accessed: Sep. 1, 2024. [Online]. Available: https://item.taobao.com/item.htm?spm=a230r.1.14.61.60076f2bbLtzCb&id=667228781819&ns=1&abbucket=16#detail

[20] *3 dBi Omni-Directional VP Antenna in 915 MHz*. Accessed: Sep. 1, 2024. [Online]. Available: https://www.amazon.com/s?k=900mhz+antenna+3dBi&crid=5DRQ899YE5B5&sprefix=900mhz+antenna+3d%2Caps%2C891&ref=nb_sb_noss

[21] *LoRa CSS PHY for GNU Radio*. Accessed: Sep. 1, 2024. [Online]. Available: https://github.com/BastilleResearch/gr-lora

[22] *IEEE 802.15.1 GFSK Transceiver for GNU Radio*. Accessed: Sep. 1, 2024. [Online]. Available: https://github.com/greatscottgadgets/gr-bluetooth

[23] *IEEE 802.11 A/g/n Transceiver for GNU Radio*. Accessed: Sep. 1, 2024. [Online]. Available: https://github.com/bastibl/gr-ieee802-11

[24] X. Guo, Y. He, Z. Yu, J. Zhang, Y. Liu, and L. Shangguan, "RF-transformer: A unified backscatter radio hardware abstraction," in *Proc. 28th Annu. Int. Conf. Mobile Comput. Netw.*, Oct. 2022, pp. 446–458.

[25] X. Guo et al., "Efficient ambient LoRa backscatter with on-off keying modulation," *IEEE/ACM Trans. Netw.*, vol. 30, no. 2, pp. 641–654, Apr. 2022.

[26] X. Guo, Y. He, J. Nan, J. Zhang, Y. Liu, and L. Shangguan, "A low-power demodulator for LoRa backscatter systems with frequency-amplitude transformation," *IEEE/ACM Trans. Netw.*, vol. 32, no. 4, pp. 3515–3527, Aug. 2024.

[27] X. Guo, Y. He, J. Zhang, Y. Liu, and L. Shangguan, "Towards programmable backscatter radio design for heterogeneous wireless networks," *IEEE/ACM Trans. Netw.*, vol. 32, no. 6, pp. 5020–5032, Dec. 2024.

[28] Y. He, Y.-M. Sun, and X.-Z. Guo, "RF computing: A new realm of IoT research," *J. Comput. Sci. Technol.*, vol. 40, no. 4, pp. 941–956, Jul. 2025.

[29] H. Zhang et al., "Terahertz sensing, communication, and networking: A survey," *IEEE Trans. Netw. Sci. Eng.*, vol. 13, pp. 1–23, 2026.

[30] Y. Zou, X. Na, X. Guo, Y. Sun, and Y. He, "Trident: Interference avoidance in multi-reader backscatter network via frequency-space division," in *Proc. IEEE Conf. Comput. Commun.*, Vancouver, BC, Canada, May 2024, pp. 1761–1770.

[31] A. Wang, V. Iyer, V. Talla, J. R. Smith, and S. Gollakota, "FM backscatter: Enabling connected cities and smart fabrics," in *Proc. USENIX NSDI*, Mar. 2017, pp. 1–34.

[32] H. Jiang, J. Zhang, X. Guo, and Y. He, "Sense me on the ride: Accurate mobile sensing over a LoRa backscatter channel," in *Proc. ACM SenSys*, 2021, pp. 125–137.

[33] M. Rostami, K. Sundaresan, E. Chai, S. Rangarajan, and D. Ganesan, "Redefining passive in backscattering with commodity devices," in *Proc. 26th Annu. Int. Conf. Mobile Comput. Netw.*, Apr. 2020, pp. 1–13.

[34] J. Jiang, Z. Xu, F. Dang, and J. Wang, "Long-range ambient LoRa backscatter with parallel decoding," in *Proc. ACM MobiCom*, Mar. 2021, pp. 684–696.

[35] T. Chakraborty et al., "Whisper: IoT in the TV white space spectrum," in *Proc. USENIX NSDI*, Renton, WA, USA, 2022, pp. 401–418.

[36] X. Guo et al., "Mighty: Towards long-range and high-throughput backscatter for drones," *IEEE Trans. Mobile Comput.*, vol. 24, no. 3, pp. 1833–1845, Mar. 2025.

[37] A. N. Parks, A. Liu, S. Gollakota, and J. R. Smith, "Turbocharging ambient backscatter communication," in *Proc. ACM Conf. SIGCOMM*, Aug. 2014, pp. 619–630.

[38] M. Badi, J. Wensowitch, D. Rajan, and J. Camp, "Experimental evaluation of antenna polarization and elevation effects on drone communications," in *Proc. 22nd Int. ACM Conf. Model., Anal. Simul. Wireless Mobile Syst.*, Miami Beach, FL, USA, Nov. 2019, pp. 211–220.

[39] M. A. Khojastepour, K. Sundaresan, S. Rangarajan, X. Zhang, and S. Barghi, "The case for antenna cancellation for scalable full-duplex wireless communications," in *Proc. 10th ACM Workshop Hot Topics Netw.*, Cambridge, MA, USA, Nov. 2011, pp. 1–6.

[40] B. Kempke, P. Pannuto, B. Campbell, J. Adkins, and P. Dutta, "Demo: PolyPoint: High-precision indoor localization with UWB," in *Proc. 13th ACM Conf. Embedded Networked Sensor Syst.*, Nov. 2015, pp. 483–484.

[41] R. Fara et al., "Polarization-based recongurable tags for robust ambient backscatter communications," *IEEE Open J. Commun. Soc.*, vol. 1, pp. 1140–1152, 2020.

[42] *Impedance Matching Definition*. Accessed: Sep. 1, 2024. [Online]. Available: https://www.analog.com/en/design-center/glossary/impedance-matching.html

Xiuzhen Guo (Member, IEEE) received the B.E. degree from Southwest University and the Ph.D. degree from Tsinghua University. She is currently an Assistant Professor with the College of Control Science and Engineering, Zhejiang University. Her research interests include wireless networks, the Internet of Things, and mobile computing. She is a member of ACM.

Long Tan (Student Member, IEEE) received the B.E. degree from Hefei University of Technology and the M.E. degree from Taiyuan University of Technology. He is currently pursuing the Ph.D. degree with the College of Control Science and Engineering, Zhejiang University. His current research interests include mobile computing and wireless networks. He is a Student Member of ACM.

Yuan He (Senior Member, IEEE) received the B.E. degree from the University of Science and Technology of China, the M.E. degree from the Institute of Software, Chinese Academy of Sciences, and the Ph.D. degree from The Hong Kong University of Science and Technology. He is currently an Associate Professor with the School of Software and BNRist, Tsinghua University. His research interests include wireless networks, the Internet of Things, pervasive, and mobile computing. He is a member of ACM.

Yuanchao Shu (Senior Member, IEEE) received the Ph.D. degree from Zhejiang University in 2015. Then, he joined Microsoft Research. He is currently a Qiushi Professor with the College of Control Science and Engineering, Zhejiang University, China. Prior to joining academia, he was a Principal Researcher at the Office of the CTO, Microsoft Azure for Operators, and the Mobility and Networking Research Group, Microsoft Research Redmond. He was a joint Ph.D. Student at the EECS Department, University of Michigan, Ann Arbor. He was a member of the organizing committee and TPC of conferences, including MobiCom, MobiSys, SenSys, SEC, IPSN, Globecom, and ICC. He received the ACM China Doctoral Dissertation Award (two years), the IBM Ph.D. Fellowship, and five best paper/demo awards from leading CS/EE conferences.

Jiming Chen (Fellow, IEEE) received the B.Sc. and Ph.D. degrees in control science and engineering from Zhejiang University, Hangzhou, China, in 2000 and 2005, respectively. He is currently a Professor with the Department of Control Science and Engineering, Zhejiang University, and the President of Hangzhou Dianzi University. His research interests include the IoT, networked control, and wireless networks. He serves on the editorial boards of multiple IEEE TRANSACTIONS and the General Co-Chair for IEEE RTCSA'19, IEEE Datacom'19, and IEEE PST'20. He was a recipient of the 7th IEEE ComSoc Asia–Pacific Outstanding Paper Award, the JSPS Invitation Fellowship, and the IEEE ComSoc AP Outstanding Young Researcher Award. He is an IEEE VTS Distinguished Lecturer. He is a Fellow of CAA.